https://doi.org/10.22226/2410-3535-2022-4-303-308

Interaction of an edge dislocation with a ⟨110⟩ tilt boundary in nickel: molecular dynamics simulation

G. M. Poletaev[†,1], Yu. V. Bebikhov[2], A. S. Semenov[2], R. Y. Rakitin[3]

[†]gmpoletaev@mail.ru

[1]Polzunov Altai State Technical University, Barnaul, 656038, Russia
[2]Polytechnic Institute of North-Eastern Federal University, Mirny, 678170, Russia
[3]Altai State University, Barnaul, 656049, Russia

The interaction of a lattice edge dislocation with a ⟨110⟩ tilt boundary in nickel was studied by the molecular dynamics method in the case when the dislocation glide plane is parallel to the grain tilt axis. The dependence of the local threshold stress on the grain misorientation angle is obtained. It is found that with increasing misorientation angle, the local threshold stress increases, but the growth rate for low- and high-angle boundaries is different: for high-angle boundaries, this growth is slower. When studying the mechanism of overcoming the low-angle ⟨110⟩ tilt boundary by an edge dislocation in the considered orientation, it was found that the dislocation, in fact, does not pass through the boundary, but exchanges places with a grain-boundary dislocation, which are ordinary perfect edge dislocations in the low-angle ⟨110⟩ tilt boundaries. When studying the interaction of a dislocation with high-angle boundaries, a peculiarity was noticed, which consists in pushing two or three grain-boundary dislocations out of the boundary at once.

Keywords: molecular dynamics, grain boundary, tilt boundary, edge dislocation.

1. Introduction

The strength and plasticity of materials essentially depend on how easily lattice dislocations can pass through grain boundaries, which are obstacles to the movement of dislocations [1–5]. In this regard, one of the topical issues is the study of the interaction between dislocations and grain boundaries, the determination of the mechanisms and factors affecting the overcoming of boundaries by dislocations.

According to one of the most common opinions, the resistance to the passage of a dislocation through the grain boundary is proportional to the difference between the Burgers vectors before and after the boundary, that is, the grain misorientation angle [1–3]. However, the results of atomistic simulation using the molecular dynamics method in [6–10] showed that the mechanism of passage of a dislocation through a grain boundary and the threshold stress depend to a large extent also on the local atomic structure of the boundary. Depending on the orientation of neighboring grains, the nature of the boundary, its specific atomic structure, and the type of dislocation, as it was found out, qualitatively different scenarios of the interaction of lattice dislocations with grain boundaries can be realized [5,11]: dislocations can be absorbed in the grain boundary without transmission of dislocations in adjacent or parent grain; dislocations can be transmitted in the adjacent grain, with or without leaving a residual dislocation in the grain boundary; absorbed dislocations at the grain boundary can be re-emitted in the adjacent grain with or without leaving a partial dislocation in the grain boundary; absorbed dislocations at the grain boundary can return to the parent grain with or without leaving a partial dislocation in the grain boundary. Due to the complex structure of many boundaries and changing conditions during plastic deformation, there are still no reliable criteria for the realization of various types of interactions between dislocations and grain boundaries. In this regard, conducting studies of individual cases, including with the help of atomistic modeling, is relevant.

In metals with a fcc crystal lattice, a significant proportion of grain boundaries are oriented along close-packed {111} planes [12,13], among which tilt boundaries with the misorientation axis ⟨110⟩ are most common [12–16]. This type of boundaries also includes twins Σ3{111}⟨110⟩, which play an extremely important role in deformation processes [17–19]. Low-angle ⟨110⟩ tilt boundaries are unique compared to other tilt boundaries — grain boundary dislocations at such boundaries are ordinary perfect edge dislocations with straight cores that do not contain jogs on them. At the tilt boundaries with other misorientation axes, for example with ⟨111⟩ and ⟨100⟩ axes, grain boundary dislocations are more complex [20].

This work is devoted to the study of the interaction of a lattice edge dislocation with a ⟨110⟩ tilt boundary by the method of molecular dynamics in the case when the dislocation glide plane is parallel to the grain tilt axis. Nickel was chosen as the metal with the fcc lattice, for which there are well-tested interatomic potentials and a large set of experimental and model data on the properties of defects of various types.

2. Description of the model

In fcc crystals, such as nickel, the {111}⟨110⟩ slip system is predominant [21]. The Burgers vector of a perfect dislocation in this case is equal to 1/2⟨110⟩, which in fcc metals, as a rule, splits into two partial dislocations 1/6⟨110⟩ separated by a stacking fault.

To simulate a moving edge dislocation, we used a computational cell in the form of a rectangular parallelepiped containing approximately 80 000 atoms with the axes oriented: X — [$\bar{1}$10], Y — [$\bar{1}\bar{1}$2], Z — [111] (Fig. 1). The XY plane in this case corresponds to the dislocation glide plane (111). To initiate the motion of the dislocation, a shear was created from the end of the computational cell. Figure 1 shows the scheme for creating a moving edge dislocation ½[$\bar{1}$01](111). The green areas from the left end moved as a whole: the upper part of the end moved along the close-packed direction [$\bar{1}$01], the lower part — along the opposite direction [10$\bar{1}$]. The displacement velocity of the upper and lower parts was constant and equal to 10 m/s. Atoms inside the green area were displaced only along the specified directions during the computer simulation. The boundary conditions on this side were thus rigid. Along the X axis, that is, along the dislocation core, the boundary conditions were set to be periodic. Conditionally rigid boundaries were used on the boundaries above and below: all atoms near the edge of the computational cell above and below in the areas highlighted in blue during the simulation were able to move only along the XY plane, movement along the Z axis was excluded. Free boundary conditions were used on the right edge of the computational cell. Such a combination of boundary conditions was sufficient to maintain, on the one hand, the given rectangular shape of the computational cell and, on the other hand, the free exit of the dislocation outside the computational cell from the right end. A similar model was used by us earlier in the study of the effect of light element impurities on the edge dislocation glide [22], as well as in [23, 24], where the motion of a dislocation was modeled.

The tilt grain boundary was created along the ($\bar{1}\bar{1}$1) plane by rotating the second crystal with respect to the first one about the [$\bar{1}$10] axis by a given angle (Fig. 1). In the present work, therefore, we considered such an orientation of a moving edge dislocation in which the glide plane of the dislocation is parallel to the boundary misorientation axis. After the removal of excess atoms, the structure was relaxed by annealing at 500 K for 20 ps, after which the computational cell was cooled to 0 K. In the process of relaxation, grain-boundary dislocations were formed at low-angle tilt boundaries.

The EAM potential from [25] was used to describe interatomic interactions in nickel in the molecular dynamics model. The experience of using this potential shows that with its help it is possible to describe various properties of nickel, including the properties of dislocations and other defects [26–28]. The simulation was carried out mainly at an initial temperature close to 0 K. As a result of the action of stresses, the computational cell was heated up to several tens of degrees during the simulation. The time integration step in the molecular dynamics method was 2 fs.

3. Results and discussion

At some point in time, the shear in the left part of the computational cell (Fig. 1) provoked the appearance of a dislocation. A perfect dislocation appeared immediately in the form of a split into a pair of Shockley partial dislocations separated by a stacking fault in the (111) plane. The splitting reaction in our case had the form: $\frac{1}{2}[\bar{1}01] \rightarrow \frac{1}{6}[\bar{2}11] + \frac{1}{6}[\bar{1}\bar{1}2]$. The distance between partial dislocations is determined, as is well known, by the stacking fault energy. In the present work, it was several nanometers, which agrees with the results of modeling by other authors, for example [23, 29]. The distance between partial dislocations, as well as the velocity of their movement, were not constant. At first, when it appeared, the dislocation "shot" from the left end (Fig. 1). Its velocity at this initial stage was the highest, about 2000 m/s, but below

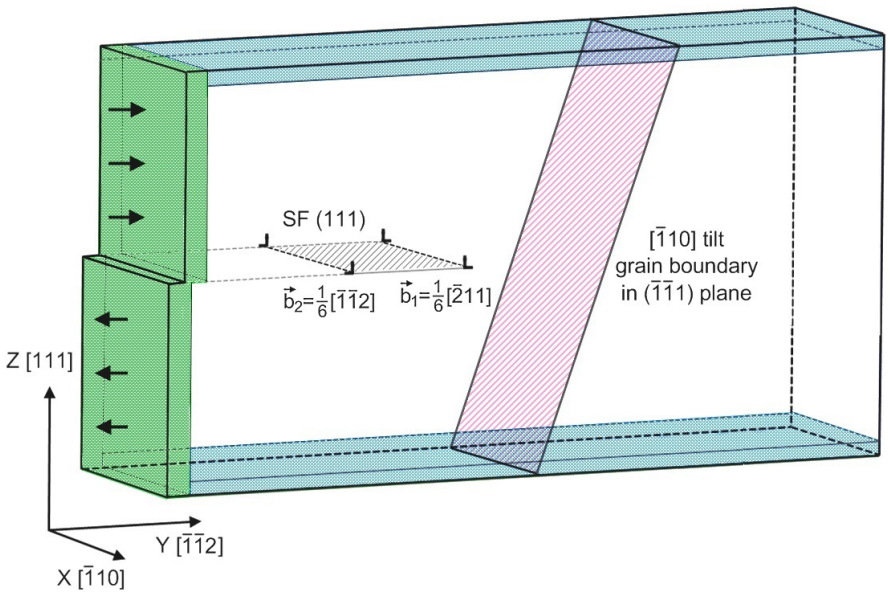

Fig. 1. (Color online) Model of interaction between an edge dislocation and a ⟨110⟩ tilt grain boundary. SF — stacking fault between partial dislocations.

the known limit, which depends on the speed of sound in the metal (5630 m/s for longitudinal waves in nickel) [29,30]. At a distance of 3–4 nm from the point of initiation, the dislocation velocity decreased, after which, as the shear continued from the left end, its sliding velocity gradually increased and then, as it approached the grain boundary, decreased again. For some time, the dislocation was stopped by the boundary until sufficient stress was accumulated for the shear to pass into the second grain.

The local threshold stress was used as a characteristic of the resistance of the boundary to the passage of an edge dislocation through it. The method of its determination was as follows. The computational domain of the computational cell was chosen, in which local stresses were concentrated when the dislocation overcame the boundary (in our work, the computational domain had the shape of a rectangular parallelepiped, whose edge length along the X axis coincided with the size of the computational cell, and the face area in the YZ plane was equal to 10.88 nm^2). Then, for a given computational domain, a graph of the potential energy was constructed during the simulation of the dislocation motion. According to the graph, the peak value of the potential energy E_{max} was determined. This value includes the energy of the lattice dislocation E_d, the activation energy a_d of overcoming the boundary by the dislocation, and the energy associated with the elastic deformation of the lattice due to the action of forces from the left end of the cell. The local threshold stress was calculated by the formula:

$$\tau = \frac{E_{max} - E_d}{S},$$

where the energies E_{max} and E_d are defined as the energies per unit width of the computational cell along the X axis; S is the area of the computational domain in the YZ plane. The value of E_d was calculated by us earlier in [19]. Potential energy and local stresses are unevenly distributed in the computational domain and have a large gradient, however, this characteristic is very indicative and is proportional to the activation energy a_d.

Figure 2 shows the dependence of the local threshold stress of overcoming the ⟨110⟩ tilt boundary by an edge dislocation in nickel on the misorientation angle at an initial temperature of 0 K. As the misorientation angle increases, the local stress increases, starting from almost zero values to several hundred MPa at large misorientation angles.

There is an opinion in the literature, for example [1–3], that the resistance to the passage of a dislocation through the grain boundary should be proportional to the difference of the Burgers vectors of the dislocation before and after the boundary: $\vec{b}_{in} - \vec{b}_{out}$. That is, according to this hypothesis, the resistance should be proportional to tan(φ/2), where φ is the misorientation angle of the tilt boundary. For comparison, in Fig. 2 overlays a graph of tan(φ/2) versus the misorientation angle, as well as a graph of the energy of the grain boundaries under consideration. The boundary energy in the model was determined as the difference between the energy of the computational cell containing the boundary and the energy of an ideal crystal containing the same number of atoms.

It should be noted that the graph of the local threshold voltage does not completely coincide with either the graph for tan(φ/2) or the graph of the boundary energy, but lies, as it were, between them. In other words, the local threshold stress does not grow linearly with increasing misorientation angle, just as the difference between the Burgers vectors of dislocations before and after the boundary (and the value of tan(φ/2)) for the considered range of angles almost increases. The growth of the local stress slows down for high-angle boundaries, but not as much as the growth of the boundary energy slows down as the misorientation angle increases. It is obvious that the qualitative difference between the structures of low- and high-angle boundaries works here, which in our case occurs approximately after an angle of 20°.

We have previously studied the interaction of edge and screw dislocations with coherent twins Σ3{111}⟨110⟩ using

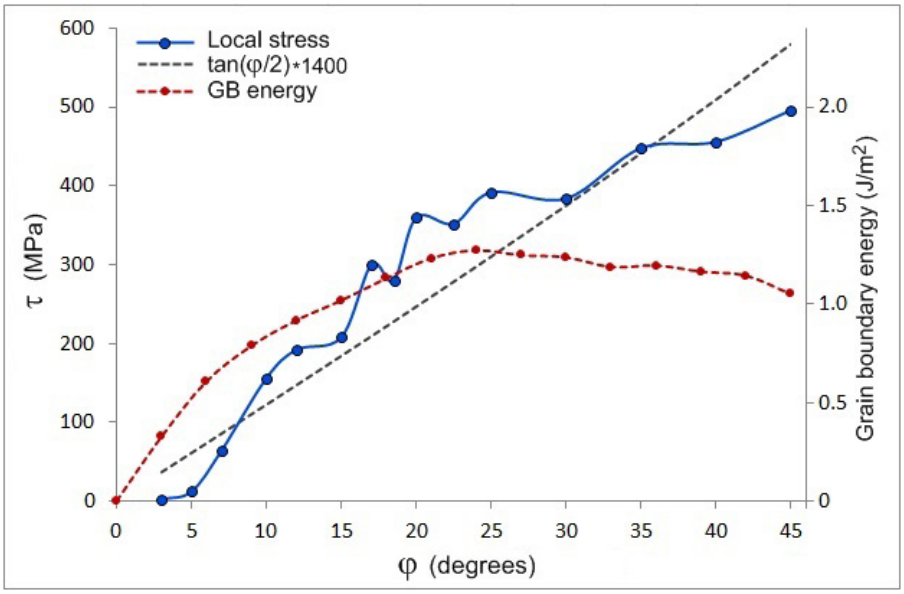

Fig. 2. (Color online) Dependence of the local threshold stress required to overcome the ⟨110⟩ tilt boundary by an edge dislocation on the misorientation angle (blue graph). For comparison, graphs of dependences of tan(φ/2) (black graph) and grain boundary energy (red graph) on misorientation angle are superimposed.

a similar model [19]. But, despite the fact that coherent twins also actually belong to ⟨110⟩ tilt boundaries, as it turned out, the mechanism of interaction with lattice dislocations for them and low-angle ⟨110⟩ boundaries differs fundamentally. A coherent twin is a serious obstacle for a moving edge dislocation. Significant stresses are required to overcome a twin by an edge dislocation [17,19,31]. The main reason is that coherent twins do not contain grain boundary dislocations, but, in fact, contain a stacking fault in the boundary plane. When the edge dislocation overcomes the twin boundary and the glide plane changes, a twinning dislocation is formed on the boundary itself, which quickly moves along the twin boundary, and if there is no obstacle for its movement, it "heals" the boundary (that is, makes it coherent again). A screw dislocation, as was clarified in [19], does not pass through the twin, but is absorbed by it, thus changing the glide plane. This occurs at much lower stresses compared to edge dislocation. After changing the slip plane, both partial dislocations diverge in different directions along the twin boundary, "healing" the boundary, as in the case of the passage of an edge dislocation.

An edge dislocation overcomes the ⟨110⟩ low-angle boundary at much lower stresses than a coherent twin. Figure 3 shows step by step the mechanism by which an edge dislocation overcomes a low-angle tilt boundary [$\bar{1}$10] with a misorientation angle of 10°. Low-angle ⟨110⟩ tilt boundaries are unique in that the grain-boundary dislocations in them are perfect dislocations that do not contain jogs, like other tilt boundaries [20]. Grain-boundary dislocations in ⟨110⟩ boundaries belong, as it were, simultaneously to slip systems on both sides of the boundary. They have short stacking faults between partial dislocations (shown as dotted blue lines in Fig. 3).

The lattice edge dislocation, as it turned out, does not pass through the boundary, but exchanges places with a grain-boundary dislocation. Moreover, the exchange of dislocations occurs even if they are in different slip planes, as in Fig. 3.

The position of the dislocation in the model was additionally monitored by the mutual displacement of the reference atoms A and B (Fig. 4 a). As the dislocation moved, a graph of the time dependence of the displacement of the A and B atoms, located under and above the slip plane of the lattice dislocation, relative to each other in the XY plane was plotted. Fig. 4 b shows an example of such a graph for the same case as in Fig. 3. On the graph, one can clearly see the moments of passage of the first and second partial dislocations (marked with numbers 1 and 2).

When a dislocation interacts with high-angle boundaries, in contrast to low-angle ones, an interesting feature appears. In general, the mechanism remains the same, that is, the lattice dislocation remains in the boundary, and the boundary emits an "extra" dislocation into another grain. But at the same time, at large misorientation angles, two, or even three, dislocations were often pushed out of the boundary at once. Figure 5 shows examples of such a phenomenon. The

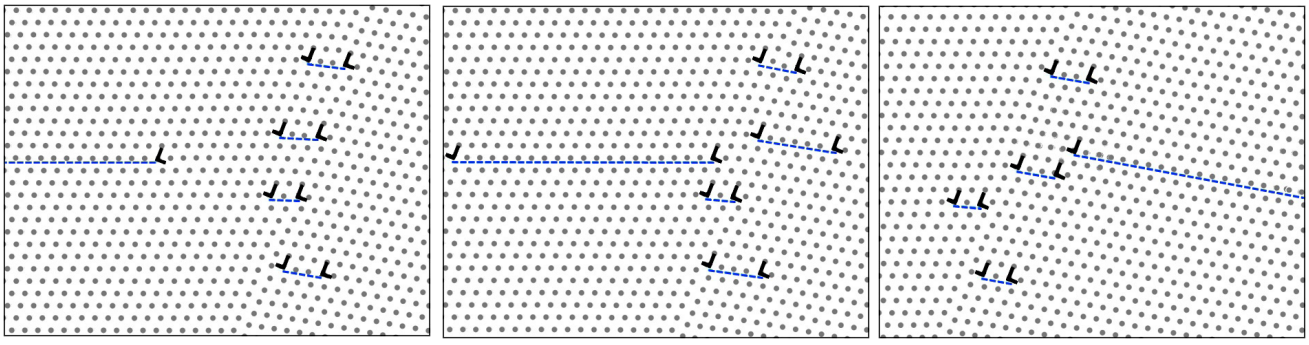

a b c

Fig. 3. (Color online) Interaction mechanism of a lattice edge dislocation with a low-angle ⟨110⟩ 10° tilt boundary: 8.5 (a), 9.5 (b), 13 ps (c). The blue dotted line shows the stacking fault between partial dislocations.

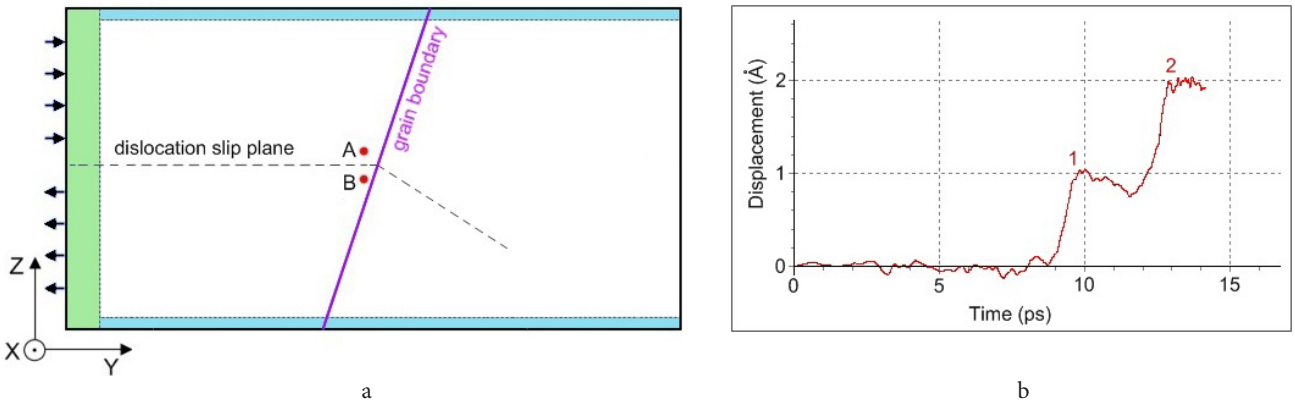

a b

Fig. 4. (Color online) Tracking the dislocation using the displacement of reference atoms: a schematic representation of the position of the reference atoms A and B (a); displacement of reference atoms relative to each other during the simulation of overcoming the 10° boundary by a dislocation: 1 and 2 in the figure are the displacements caused by the passage of the first and second partial dislocations (b).

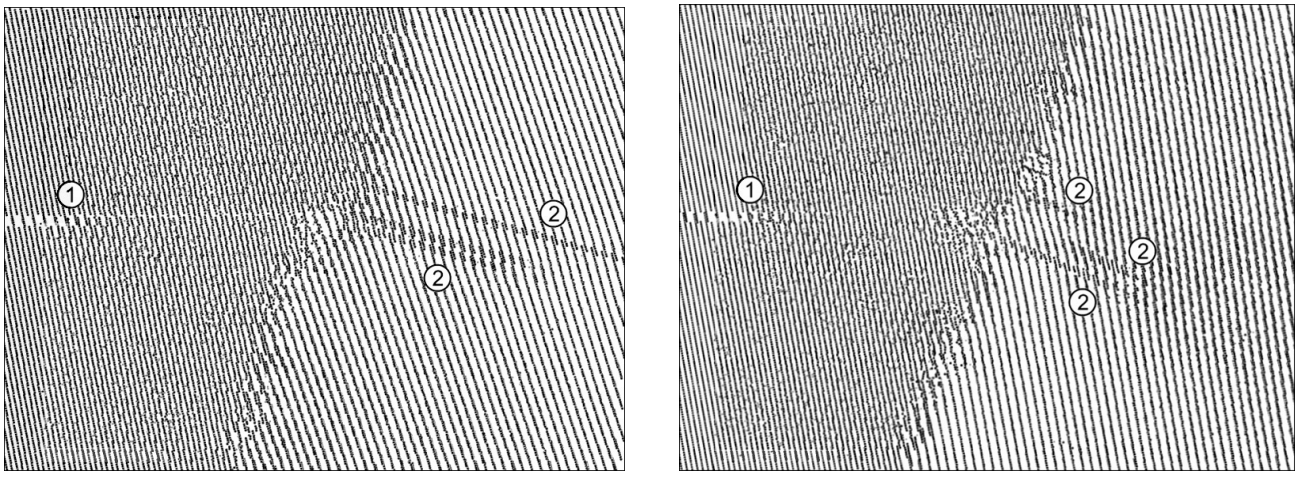

a b

Fig. 5. Examples of separation of several dislocations from the high-angle ⟨110⟩ boundary at once: 17°, 32 ps (a); 25°, 33.5 ps (b). 1 — plastic shear from the left end, 2 — dislocations released by the boundary. The computational cells are oriented in such a way that the dislocations can be seen better.

bands in the figure, along which the shear is clearly visible, are stacking faults between partial dislocations.

As the misorientation angle increases, the density of grain-boundary dislocations increases, but the Burgers vector of each dislocation does not change and remains in our case approximately equal to the vector of perfect dislocation. The emission of several dislocations at once from high-angle boundaries in this case, apparently, is explained by their relatively high mobility, while the appearance of a new dislocation from the left end of the computational cell requires significantly more energy. Due to the shear of the upper and lower parts of the computational cell on the left end, internal stresses are formed that provoke the formation of a dislocation not only on the left end of the cell, but also the emission of dislocations from the grain boundary even without the participation of an external dislocation.

4. Conclusion

The interaction of a lattice edge dislocation with a ⟨110⟩ tilt boundary in nickel was studied by the molecular dynamics method in the case when the dislocation glide plane is parallel to the grain tilt axis. The dependence of the local threshold stress on the grain misorientation angle is obtained. It is found that with increasing misorientation angle, the local threshold stress increases, but the growth rate for low- and high-angle boundaries is different: for high-angle boundaries, this growth is slower.

When studying the mechanism of overcoming the ⟨110⟩ tilt boundary by an edge dislocation in the considered orientation, it was found that the dislocation, in fact, does not pass through the boundary, but exchanges places with the grain-boundary dislocation, which are ordinary perfect edge dislocations in the ⟨110⟩ tilt boundaries. In this case, the lattice dislocation remains in the boundary, while the grain-boundary one is "released" and goes into the second grain. When studying the interaction of a dislocation with high-angle boundaries, a peculiarity was noticed, which consists in pushing two or three grain-boundary dislocations out of the boundary at once.

References

1. T. C. Lee, I. M. Robertson, H. K. Birnbaum. Metallurgical Transactions A. 21, 2437 (1990). Crossref
2. Sh. Kondo, T. Mitsuma, N. Shibata, Y. Ikuhara. Science Advances. 2, e1501926 (2016). Crossref
3. H. Pan, Y. He, X. Zhang. Materials. 14 (4), 1012 (2021). Crossref
4. M. Hamid, H. Lyu, B. J. Schuessler, P. C. Wo, H. M. Zbib. Crystals. 7 (6), 152 (2017). Crossref
5. F. Javaid, H. Pouriayevali, K. Durst. Journal of Materials Research. 36, 2545 (2021). Crossref
6. Y. Cheng, M. Mrovec, P. Gumbsch. Philosophical Magazine. 88 (4), 547 (2008). Crossref
7. M. Dupraz, Zh. Sun, C. Brandl, H. Van Swygenhoven. Acta Materialia. 144, 68 (2018). Crossref
8. M. P. Dewald, W. A. Curtin. Modelling and Simulation in Materials Science and Engineering. 15 (1), S193 (2007). Crossref
9. C. Brandl, E. Bitzek, P. M. Derlet, H. Van Swygenhoven. Applied Physics Letters. 91 (11), 111914 (2007). Crossref
10. D. V. Bachurin, D. Weygand, P. Gumbsch. Acta Materialia. 58 (16), 5232 (2010). Crossref
11. E. Bayerschen, A. T. McBride, B. D. Reddy, T. Bohlke. Journal of Materials Science. 51 (5), 2243 (2016). Crossref
12. J. Li, S. J. Dillon, G. S. Rohrer. Acta Materialia. 57 (14), 4304 (2009). Crossref
13. S. Ratanaphan, D. L. Olmsted, V. V. Bulatov, E. A. Holm, A. D. Rolletta, G. S. Rohrer. Acta Materialia. 88, 346 (2015). Crossref
14. D. L. Olmsted, S. M. Foiles, E. A. Holm. Acta Materialia. 57 (13), 3694 (2009). Crossref
15. V. V. Bulatov, B. W. Reed, M. Kumar. Acta Materialia. 65, 161 (2014). Crossref
16. M. A. Tschopp, Sh. P. Coleman, D. L. McDowell. Integrating Materials and Manufacturing Innovation. 4, 176 (2015). Crossref
17. N. V. Malyar, B. Grabowski, G. Dehm, C. Kirchlechner. Acta Materialia. 161, 412 (2018). Crossref

18. Y. Liang, X. Yang, M. Gong, G. Liu, Q. Liu, J. Wang. Computational Materials Science. 161, 371 (2019). Crossref
19. C. Chen, F. Zhang, H. Xu, Z. Yang, G. M. Poletaev. Journal of Materials Science. 57, 1833 (2022). Crossref
20. G. M. Poletaev, I. V. Zorya, R. Y. Rakitin. Letters on Materials. 10 (4s), 543 (2020). Crossref
21. J. P. Hirth, J. Lothe. Theory of Dislocations. 2nd ed. New York, Wiley (1982) 857 p.
22. G. M. Poletaev, I. V. Zorya. Journal of Experimental and Theoretical Physics. 131 (3), 432 (2020). Crossref
23. D. Rodney, L. Ventelon, E. Clouet, L. Pizzagalli, F. Willaime. Acta Materialia. 124, 633 (2017). Crossref
24. C. Chen, F. Meng, P. Ou et al. Journal of Physics: Condensed Matter. 31, 315701 (2019). Crossref
25. G. P. Purja Pun, Y. Mishin. Philosophical Magazine. 89, 3245 (2009). Crossref
26. G. M. Poletaev. Journal of Experimental and Theoretical Physics. 133, 455 (2021). Crossref
27. G. M. Poletaev, I. V. Zorya, M. D. Starostenkov. Journal of Micromechanics and Molecular Physics. 3 (1&2), 1850001 (2018). Crossref
28. G. M. Poletaev, I. V. Zorya. Technical Physics Letters. 46 (6), 575 (2020). Crossref
29. Sh. Zhao, Yu. N. Osetsky, Y. Zhang. Journal of Alloys and Compounds. 701, 1003 (2017). Crossref
30. G. Po, Y. Cui, D. Rivera, D. Cereceda, T. D. Swinburne, J. Marian, N. Ghoniem. Acta Materialia. 119, 123 (2016). Crossref
31. Y. Liang, X. Yang, M. Gong, G. Liu, Q. Liu, J. Wang. Computational Materials Science. 161, 371 (2019). Crossref